A simulation model of the pulse returns for a short-range SAS

Peter T. Gough and Michael P. Hayes
Department of Electrical and
Computer Engineering
University of Canterbury
Christchurch, New Zealand 8140
Email: {peter.gough, michael.hayes}@canterbury.ac.nz
Telephone: [+64] 3 364–2297
Fax: [+64] 3 364–2761

***Abstract*— Numerical simulations of sub-marine acoustical experiments can often save significant sea-time but to have any value, the simulation needs to produce believable results. This paper looks at a simple acoustic simulation which relies on the scattering surface (the seafloor) being approximated by a collection of sub-wavelength smooth rectangular facets. The experiment being modeled is a monostatic, pulse-echo sonar working in extremely shallow water (<2m in depth). Various modifications to the model of the seafloor are explored to see what assumptions and approximations influence the seafloor reverberation. Volume reverberation from the underlying sediments is not considered. The motivation for this work is to see how feasible it is to operate a broad-beam, broad-band synthetic aperture sonar in extremely shallow waters so a significant part of this investigation is to measure how the phase of the pulse echo evolves as the sonar head tracks over the rough seafloor under extreme reverberation conditions. Our conclusion is that the model is useful for small seafloor areas but not for large surface areas which require too much computation.**

I. Introduction

In investigations that involve the interaction of sound waves with the seafloor, there are several contributing factors to the way the incident sound wave is reflected and scattered. The incident sound wave may be planar or spherical, pulsed or continuous, the seafloor may be smooth or rough, there may be volume scattering in the sea column and scattering from the seafloor sediments, and if the seafloor is rough enough, there may be layover, shadowing and multiple reflections. Compounding the problem in very shallow waters (<2m) is the seafloor-sea surface multipath. The emphasis in this paper is modeling sound interaction of the sea/seafloor interface where the sonar head may be less than 0.5m from the seafloor. The motivation behind this modeling to to investigate the feasibility of operating a synthetic aperture sonar (SAS) in extremely shallow waters.

All of the complicating factors make constructing an analytic model of the actual physical environment daunting in its complexity and so workable models are mostly restricted to simple seafloor scattering with no layover, no shadowing, no multiple reflections and no multipath. Many of these mathematical and numerical models are narrow band, they commonly resort to the high frequency limit and are often further restricted to small incidence and scattering angles. Even so many of the models still only predict the expected value of the target strength rather than the detailed amplitude and phase structure of the returned time-domain echo given some specific seafloor profile. To get an example of a typical echo return, it is usually necessary to compute the echo return based on some type of simulation model. Since we are more interested in the ping-to-ping coherence as the sonar moves over the seafloor, we are less concerned as to the accuracy of the rough surface target strength which has been the focus of much prior work [2], [3].

The organization of this paper is as follows. Firstly there is a discussion of the types of surface and seafloor models. The mathematical description of the rough surface scattering process used here is based on the Kirchhoff approximation of the Kirchhoff Fresnel integral. Then there is a discussion on how a realistic pulse waveform is simulated to include any frequency weighting effects of real projectors and real hydrophones. Four 3m by 3m "seafloors" are used for the simulations: a mirror surface, a granular flat surface, a rough surface with a Gaussian spectral density and an equally rough surface with a power-law spectral density. The last two surface have approximately the same RMS height variation over the 3m by 3m surface and similar autocorrelation distance. The mirror surface was used to check that the surface and temporal sampling rates were sufficient to avoid any aliasing over the area modeled. With that several returns are simulated to show the effects of roughness on the backscattered channel impulse response. Then the actual backscattered echo returns are simulated to see how the amplitude and phase of the narrow band signal evolve with delay time and as the sonar tracks over the simulated seafloor.

II. Simulation models

Many computer models of the sea to seafloor interface assume a single-valued seafloor height with no multiple scattering. Basically there are two approaches to modeling a single-valued seafloor. The simplest is a "cloud of points" model where the seafloor is sampled in x and y with a 2-D spatial sample spacing of Δx and Δy some small fraction

978-1-4244-5222-4/10/$26.00 ©2010 IEEE

of a λ (more on that later) with the value of $z(x, y)$ being the height variation from the mean seafloor at x, y. The big disadvantage of this approach is the increase in computing time required as the seafloor area increases.

A second approach is to use a tesselated collection of larger conjoined triangular facets; each of which may be many wavelengths in extent. A slight modification to this large facet model is where each facet might have it own roughness parameter [1]. Although the number of facets in the large facet-based model is far fewer in number than the number of individual sample points in a "cloud of points" model, the necessity to compute an irregular aperture diffraction pattern make this a more complicated model to code. However, the extra effort may still be worth the effort if there are large specular objects or extensive simulation work anticipated. However in this current paper we concentrate of the simpler "cloud of points" model so as to understand its limitations and some of the slight modifications needed to make it more realistic.

III. The "cloud of points" model

The "cloud of points" model has the great benefit of simplicity and it can easily incorporate spreading losses and absorption in the water column as well as any non-constant velocity profile. The idea is that each of the sample points that makes up the seafloor, re-radiates a proportion of its incident energy at an appropriate amplitude and phase and this re-radiated "wavelet" is picked up by a hydrophone after a suitable delay. Provided the process is linear (which also assumes the surface is not too rough, there is no layover or multiple scattering), the signal received by the hydrophone is the linear sum of all the reradiated wavelets.

A convenient place to start is with a complete mathematical description of the equivalent continuous process (i.e., when the separation between the points shrinks to zero). So we take an homogeneous, source-free volume bounded by a surface S with the acoustic potential ψ inside the volume at a point located at $\mathbf{x}$ for a specific frequency f and described by the Kirchhoff-Helmholtz integral (KHI);

$$\begin{aligned} \psi(\mathbf{x}, f) \quad &= \quad \iint_{\Omega} \left(G(\mathbf{x}' - \mathbf{x}, f) \cdot \frac{\partial}{\partial \hat{\mathbf{n}}} \psi(\mathbf{x}', f) \right. \\ &- \quad \left. \psi(\mathbf{x}', f) \cdot \frac{\partial}{\partial \hat{\mathbf{n}}} G(\mathbf{x}' - \mathbf{x}, f) \right) \, \mathrm{d}\Omega(\mathbf{x}') \quad (1) \end{aligned}$$

where G is the free space Green's function and $\hat{\mathbf{n}}$ is the local normal on the surface S. Common usage has the non-zero part of the acoustic potential on the surface define the extent of the aperture Ω in (1) with $\mathbf{x}'$ a point located on Ω and substitutes $d\Omega(\mathbf{x}')$ by $d\Omega$ (which has units of m^2). Equation (1) computes the amplitude and phase of the field at a point $\mathbf{x}$ inside the volume from the acoustic potential and its normal derivative at the aperture Ω and it accounts for occlusions as well as multiple scattering from one part of the aperture to another.

Much of the acoustic modeling is concerned with reflections and scattering from a surface interface rather than transmission through an aperture so without loss of generality, we now consider Ω to be a reflecting and scattering surface. The solution of (1), regardless of the choice of Green's function, is far from simple and there are only a few analytic solutions available restricted to rather simple apertures/surfaces (e.g., flat, annular). Although mathematically exact numerical solutions do exist for other more complicated surfaces, they are sufficiently time consuming to compute that it is common to collapse the 2-D scattering surface into a 1-D line equivalent [2] [3] which limits the surfaces under consideration to those with isotropic power spectra. However many of the numerically "exact" 1-D solutions (exact to the extent that no approximations are applied) are used to test the validity of various simplifying approximations of the 2-D surface.

Probably the most widely used simplifying assumption is the Kirchhoff approximation (KA) which enforces linear superposition on the mathematics of (1). Basically the KA assumes the field and its derivative at the aperture would be the same whether the surface was there or not. This requires that there is (i) no shadowing of the surface and (ii) no scattering from one part of the surface to another part. With some simple projection arguments, the KA can be extended to account for some shadowing of the surface but this modification is normally limited to the higher frequencies since diffraction from edges, peaks and ridges of the surface would fill in the shadow regions at lower frequencies. (In the KA high-frequency limit, each facet acts like a small mirror with no diffraction at all and so the scattered field at the receiver only has contributions from facets that happen to have $\theta_i = \theta_s$ relative to the local surface normal of the facet [4], p357. The main value of the KA high frequency limit is to estimate the target strength of a rough seafloor close to the specular angle.) More importantly the surface must be sufficiently smooth so that there is little scattering along the plane of the surface. This is enforced by requiring that the radius of curvature of all parts of the rough surface be large compared to λ or more recently, that the correlation distance in the horizontal plane to be many wavelengths [2].

An additional limitation is the need to restrict the incident angles to less than any critical incident angle for the seafloor. Fast dense seafloors (e.g., sand) have a critical angle of incidence where there is some energy contained in the non-propagating evanescent wave. As this energy interacts with the down range surface roughness, it reradiates causing a noticeable increase in the backscattered energy. There is clear evidence of this enhanced backscatter around the critical angle [4] p337 and this is not modeled at all using the KA.

So on the assumption that the KA can be applied without significant errors, how can (1) can be simplified enough to produce useful analytic or numerical results from any rough surface realisation? Traditionally the KHI is simplified to the Kirchhoff-Fresnel diffraction integral (KFI) by using $\exp(-jkr)/4\pi r$ as the free-space Green's function. This results in a frequency-weighted KFI as

$$E(\mathbf{x},f) = S(f)\cdot H(\mathbf{x},f) \quad \text{with}$$
$$H(\mathbf{x},f) = \iint_{\Omega} \mathcal{R}_{\Omega}\frac{\exp(-\mathrm{j}k(r_i+r))}{(4\pi)^2 r_i r}\cdot$$
$$\left(\left(\mathrm{j}k+\frac{1}{r_i}\right)\cos(\mathbf{r_i},-\hat{\mathbf{n}})+\left(\mathrm{j}k+\frac{1}{r}\right)\cos(\mathbf{r},\hat{\mathbf{n}})\right)\mathrm{d}\Omega \quad (2)$$

where $E(\mathbf{x},f)$ is the output voltage of the hydrophone and proportional to the acoustic potential at the hydrophone $\psi(\mathbf{x},f)$, $S(f)$ the spectrum of the projector/ hydrophone combination, $H(\mathbf{x},f)$ is the spectrum of the channel impulse response, $\mathcal{R}_{\Omega}$ is reflection coefficient of the surface at the angle of incidence, k is the wavenumber, r_i the scalar distance from the projector to a location in the surface, r the scalar distance from the same location in the surface to the hydrophone, and where $\cos(\mathbf{r_i},-\hat{\mathbf{n}})$ the cosine of the angle between the incident ray $\mathbf{r_i}$ and the local surface normal $\hat{\mathbf{n}}$ (which we define as pointing towards the projector), $\cos(\mathbf{r},\hat{\mathbf{n}})$ the cosine of the angle between the local surface normal and the ray from the surface to the hydrophone $\mathbf{r}$.

In the monostatic, flat surface, back-scattering problem where the projector and the hydrophone are co-located, symmetry above and below the reflection plane can be used to simplify (2) still further since $\mathbf{r}=-\mathbf{r_i}$. This means the KFI for back-scattering rough surfaces can be reduced to [1] (and from here on the location $\mathbf{x}$ dependence of both E and H are dropped)

$$\begin{aligned} H(f) &= \iint_{\Omega}\mathcal{R}_{\Omega}\frac{\exp(-\mathrm{j}k2r)}{(4\pi r)^2}\cdot 2\,(\mathrm{j}k+1/r)\cdot\cos(\mathbf{r},\hat{\mathbf{n}})\cdot\mathrm{d}\Omega \\ &= \iint_{\Omega}\mathcal{R}_{\Omega}\frac{\exp(-\mathrm{j}k2r)}{(4\pi r)^2}\cdot 2\,(\mathrm{j}k+1/r)\cdot\cos\theta_i\cdot\mathrm{d}\Omega \quad (3)\end{aligned}$$

where θ_i is the local angle of incidence and $\mathcal{R}_{\Omega}$ represent the reflection coefficient of the surface at that angle. For a pressure release interface such as the sea surface, the reflection coefficient $\mathcal{R}_{\Omega}=-1$ for all angles of incidence. However for the seafloor, the plane wave reflection coefficient depends on the local angle of incidence, the density ρ and speed of sound c of the sediment compared to the water above. When the sediment is modeled as a lossy elastic or poroelastic material capable of supporting shear waves or the sediment has significant absorption, then $\mathcal{R}_{\Omega}$ become complex but unless otherwise specified, we are assuming a simple lossless fluid-like sediment. For sandy sea floors, the density and speed of sound are greater than those in the sea water above so the transmitted wave is refracted away from the surface normal in which case there is a critical angle. Above the critical angle, $\mathcal{R}_{\Omega}\approx 1$ so no energy propagates into the sediment (i.e., there is total internal reflection) and all the energy is either coherently scattered in the specular direction or non-coherently scattered back into the full upper hemisphere. Consequently around $\theta_i=\theta_c$, the KFI with the KA **underestimates** the backscattering strength of the rough surface.

In shallow waters, the predominance of fine silt/mud as well as biological activity in the top layers of sediment sometimes makes the speed of sound less than that of the water above and the wave transmitted into the sediment is refracted towards the surface normal. Under these circumstances, the reflection coefficient $\mathcal{R}_{\Omega}<1$ for all θ_i and there is no critical angle. Instead there is an angle of intromission where all the incident energy at this incidence angle is refracted into the sediment. However this is accounted for in the reflection coefficient $\mathcal{R}_{\Omega}$ and so the KFI is calculated correctly. Figure 1 shows plots of the absolute value of the reflection coefficients for both fast and slow sediments which can support shear waves. In this figure, c_P is the speed of the compressional wave and c_S that of the shear wave.

One aspect of shallow water sediments that has caused some us some concern in out tank experiments is what we believe are air bubbles trapped in the top few wavelength of the sediment. To see how these bubbles might change the plane wave reflection coefficient, we assume the bubbles are the equivalent of a contiguous layers of air 50 nm thick on top of the sediment. It is surprising how a thin layer of air at the interface causes such a significant change in the reflection coefficient. This is shown in Fig. 2 where the 50nm layer of air on the surface of the sediment changes the reflection coefficient dramatically especially the phase shift at normal angles of incidence. Whether it is appropriate to model a random distribution of sub-wavelength bubbles as a single contiguous surface layer is an open question.

A final comment on the use of the plane wave reflection coefficient in computing the KFI for extremely shallow waters. When the seafloor is flat and the sonar is close to the seafloor, it may be appropriate to modify the reflection coefficient to that appropriate for a spherical incident wave [8]. However, for a rough seafloor modeled as contiguous 2-D array of sub-wavelength facets, the size of the facet is sufficiently small that the incident wavefront would appear to be planar even when the distance of the sonar from the seafloor is only a few tens of wavelengths.

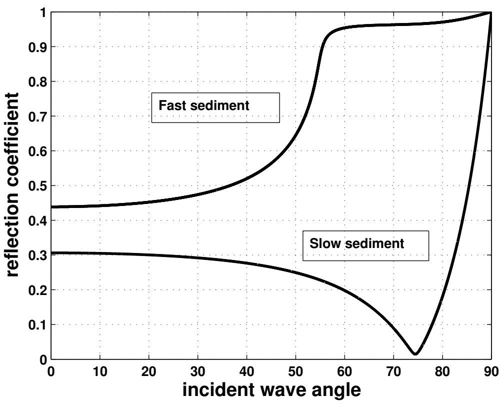

Fig. 1. The absolute values of the plane wave reflection coefficients for lossy elastic sediments. For both plots $\rho=1\,\mathrm{kgm}^{-3}$, $c=1496\,\mathrm{ms}^{-1}$ water with $\rho=2.1\,\mathrm{kgm}^{-3}$ and shear wave velocity $c_S=120\,\mathrm{ms}^{-1}$ for the sediment. The fast sediment has a $c_P=1770\,\mathrm{ms}^{-1}$ and the slow sediment has a $c_P=1300\,\mathrm{ms}^{-1}$.

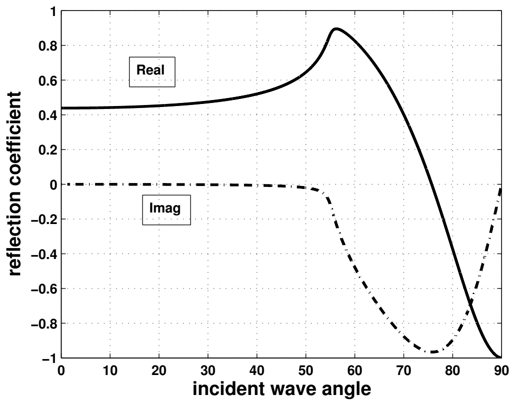

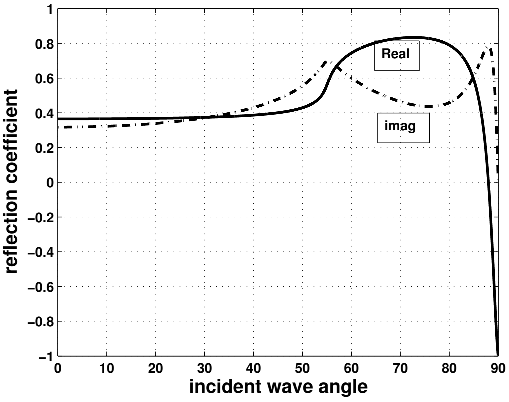

Fig. 2. The complex plane wave reflection coefficients for a fast sediment with a thin air layer on top of the sediment. For both plots the sediment has $\rho = 2.1\,\mathrm{kgm}^{-3}$ and $c = 1770\,\mathrm{ms}^{-1}$. (a) No air layer. The absolute value of this plot would be the same as the fast sediment in Fig.1. (b) The complex reflection coefficient with a surface air layer 50nm thick.

There has been some discussion about the need to use the local surface normal $\hat{\mathbf{n}}$ in the KFI (3). Clearly in the high frequency limit or when only a small area of the seafloor is illuminated by a pencil beam, it is appropriate. However in the low frequency limit or when large areas are illuminated by wide beam-width transducers, $\cos(\mathbf{r}, \hat{\mathbf{z}})$ has been substituted for $\cos(\mathbf{r}, \hat{\mathbf{n}})$ [9] apparently without error. A similar simplification also works for the reflection coefficient. For backscatter, we can apply $\mathcal{R}_\Omega$ at the angle of incidence to the mean seafloor normal $\hat{\mathbf{z}}$ since at any instance in time, the combined pulse echo response comes from an annulus of the seafloor which covers many facets. Although a single facet inside any particular annulus has a local angle of incidence, these average to that of the mean angle of incidence. Thus for backscatter it is unnecessary to calculate the local angle of incidence for each facet; it is merely enough to calculate the mean angle of incidence to the seafloor for a facet at that slant range.

There are many relevant papers that include the beam-patterns of the projector and the hydrophone; see for example [6], but here we are assuming wide beam-width or even omni-directional projector and hydrophone beam-patterns to keep

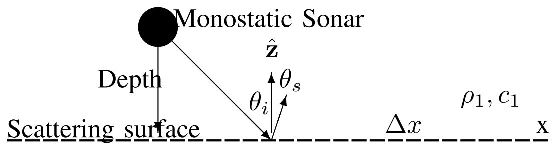

Fig. 3. Replacing the "cloud of points" with elemental flat rectangular facets.

the important mathematics as simple as possible. Also with a monostatic sonar where a single transducer is used for both transmission and reception, the transmitted waveform must be time-gated or chirped so as to separate the transmitted signal from the returned echoes.

[*An additional simplification of (3) occurs if $S(f)$ is band-limited and has no contribution around DC. Under these circumstances, $k > 1/r$ for all radiated frequencies and*

$$E(f) \approx S(f) \cdot \iint_\Omega \mathcal{R}_\Omega \frac{\exp(-\mathrm{j}2kr)}{(4\pi r)^2} \cdot 2\mathrm{j}k \cdot \cos\theta_i \cdot \mathrm{d}\Omega, \quad (4)$$

however, we will retain the $1/r$ term inside the integral for the time being.]

In the time domain, the Fourier transform of the spectrally weighted integral equation becomes

$$e(t) = \iint_\Omega \frac{\mathcal{R}_\Omega}{(4\pi r)^2} \cdot \left(\frac{ds(t - 2r/c)}{dt} + \frac{s(t - 2r/c)}{r} \right) \cdot \cos\theta_i \cdot \mathrm{d}\Omega \quad (5)$$

where $e(t)$ is the combined wave as received by the hydrophone (with $t = 0$ the start time of pulse transmission) and is the inverse FT of $E(f)$, $s(t)$ is the transmitted waveform shaded by the frequency responses of the projector and hydrophone and is the inverse FT of $S(f)$.

A. The amplitude and cosine factors of the re-radiated wavelets

A small conceptual problem with the simple "cloud of points" seafloor model is that a point has no area and therefor intercepts no incident power and so consequently re-radiates no power and this is clearly not the case. So a slightly more realistic model assumes each sample point in the x, y plane represents a small flat rectangular facet with area $d\Omega = \Delta x \times \Delta y$ that is insonified by the incident wavefront and re-radiates the incident power (or an appropriate proportion thereof depending on the assumed bulk reflection coefficient) from a point source located at the sample point x, y, z. In shallow water when either the projector and/or the hydrophone is close to the seafloor as implied in Fig.3, the incidence and reflected/scattered angles do not obey the small angle restriction (i.e., $\cos\theta \ncong 1$) and the re-radiated wavelets need to incorporate some angular dependance into the amplitude factor. If we first consider the active sonar equation in its monostatic non-logarithmic form, we get the far-field scattered power density of the selected target at the receiving hydrophone as

$$P_r = \mathbf{P}_t \cdot G_t \cdot \frac{1}{4\pi r^2} \cdot \sigma \cdot \frac{1}{4\pi r^2} \qquad (\mathrm{Wm}^{-2}) \quad (6)$$

where $\mathbf{P}_t$ is the transmitted power in W, G_t is the gain of the transmitting projector (assumed equal to unity for an omnidirectional projector), r is the range in m and σ is the sonar scattering cross sectional area of the target in m^2 as seen from the direction of the incident wavefronts.

If the target is a single isolated sphere, then the sonar back scattering cross-section σ is independent of illumination angle but shows significant variation as a function of frequency. In the Rayleigh region where the diameter of the sphere is smaller than a wavelength, σ varies as k^4. In the "optical" region, where the diameter is much larger than a wavelength, σ is asymptotic to the physical cross-sectional area of the sphere. In between is the resonance region where the diameter of the sphere is of similar size to the wavelength and resonant effects make the sonar cross section σ vary from something like twice its physical cross section to half its physical cross section. Interestingly there is little experimental evidence of the backscattering target strength having a k^4 dependence even when the size of the individual scattering centres is less than a wavelength [5] so treating the seafloor as a cloud of independent sub-wavelength spherical scatterers is questionable.

However for this paper, we assume the seafloor is modeled, not as an array of small spheres but as an array of small rectangular flat facets with area $d\Omega$. Since an individual facet has aspect angle dependence, there should be some angular variation of the sonar back-scattering cross section σ. So now consider the situation of a single, isolated, rectangular, flat plate floating in free space. To a first approximation the amount of power this elemental plate intercepts is proportional to $\cos\theta_i$ the angle between the ray direction of the incident wavefront and the surface normal as shown in Fig.3. The re-radiated power would be a maximum close to the surface normal and would have to fall to zero along the horizontal plane of the facet and so the back-scattering cross section σ, as given by [6], is

$$\begin{aligned} \sigma &\propto \left(\frac{\sin(k\,\Delta x \sin\theta_i)\cos\theta_i}{\Delta x \sin\theta_i}\right)^2 \\ &\approx k^2\cos^2\theta_i \end{aligned} \tag{7}$$

for low frequencies or small angles of incidence.

Since the far field back-scattered power density is proportional to k^2 times $\cos^2\theta_i$, it is reasonable to conclude that the back-scattering amplitude of a wavelet from a facet in the aperture is proportional to k times $\cos\theta_i$. The justification of a $k\cdot\cos\theta_i$ dependence of the amplitude factor which we garnered from the sonar equation (6) and (7) is clearly in agreement with the $k\cdot\cos\theta_i$ factor inside the KFI of (3). Thus it seems eminently reasonable to conclude from two different arguments that there is indeed a $k\cdot\cos\theta_i$ dependence on the far field amplitude factor of all samples of the seafloor even when it is represented as a discrete facet in a "cloud of points" model of the seafloor.

B. The simulated transmitted signal $s(t)$

Although it is common to transmit a swept-frequency chirp signal and then pulse compress the received echoes, this will not be necessary here. For many experiments, the sonar is reverberation-limited rather than noise-limited and so we are not restricted by peak-power problems of the projector. However since we need a reasonable range resolution we do need to transmit a short length pulse with a reasonable bandwidth and we have found experimentally that three cycle pulse at 80kHz, the centre frequency of the transducer available, is quite feasible. Since it was important to simulate the future experimental setup as closely as possible, the $s(t)$ needed to represent not only the transmitted waveform sent by the power amplifier to the projector but also any frequency shading applied by the physical construction of projector and hydrophone. To that end, a preliminary experiment was set up with two identical omni-directional transducers spaced exactly 0.96m apart. The three cycle 80kHz pulse was transmitted on one transducer and received by the other. Since this experimental waveform has some noise , the waveform was then decomposed into a collection of exponentially damped sinusoids using the pencil matrix method. The waveform $s(t)$ used in all the subsequent simulated experiments was reconstituted with the most significant 14 of the damped sinusoids resulting in the waveform $s(t)$ and its differential shown in Fig. 4(a) and the corresponding amplitude spectrum $|S(f)|$ shown in Fig. 4(b) Once the appropriate transmitted waveform $s(t)$ has been created, it is necessary to differentiate it to provide the correct delayed re-radiated wavelet for each seafloor sample.

C. The seafloor power spectrum

So far there has been an assumption in the "cloud of points" model that the z displacement of each point is uncorrelated between adjacent points which is clearly untrue for any real seafloor. A common assumption is that not only is the amplitude of the displacement $z(x, y)$ Gaussianly distributed but the spatial power spectrum (and so autocorrelation function) are also Gaussian. One of the advantages of assuming a Gaussian spatial power spectrum is that we can often use the Kirchhoff approximation to predict backscattered target strength as a function of incidence and of scattering angle [2]. Regardless of the spatial correlation, the seafloor needs to be "rough". In the Rayleigh sense, this implies that the RMS height variation around the mean needs to be $> \lambda/8$. If we set the RMS height variation of our simulated surface to be 1cm then the surface would be considered "rough" to all frequencies above 20kHz.

One of the parameters of the seafloor we need to know is the RMS slope angle which, for the Gaussian surface shown in Fig.5, is

$$\gamma = \tan^{-1}(\sqrt{2}h/l) \approx 25^\circ \tag{8}$$

where h is the RMS height variation from the mean surface and l is the surface correlation length. This means that there should be little self shadowing up to an incidence angle of 15° but beyond that and increasing % of the surface will

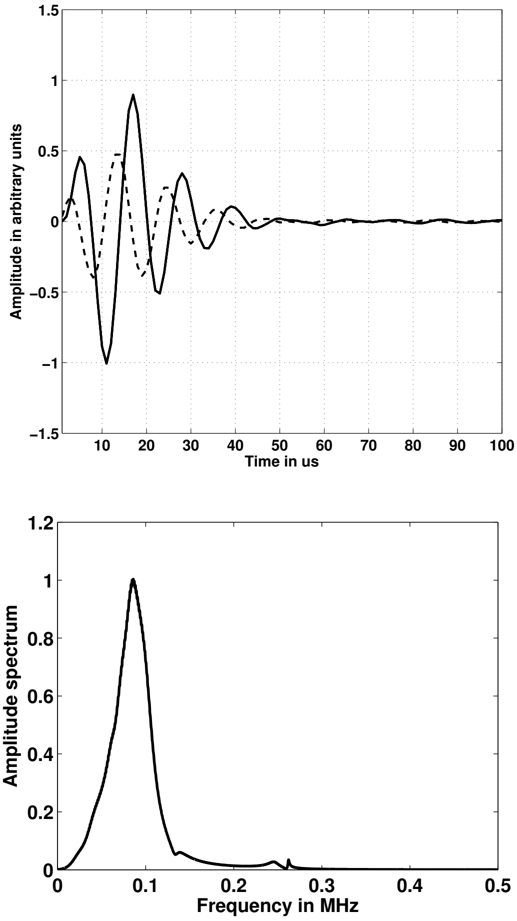

Fig. 4. The transmitted waveform as used in the simulator. (a) The waveform s(t) as defined below (5) accounts for all the spectral shading of both the transmitting projector and receiving hydrophone but without the noise of the experimental waveform. The dotted line is the differential of $s(t)$. (b) Its amplitude spectrum $|S(f)|$ where the y axis scaling is arbitrary.

suffer some shadowing and results using the KA will become increasing inaccurate.

There is ample evidence that a natural surface such as sandy or mud/silt seafloor obeys a power law spatial spectrum so that there is a two dimensional autocorrelation function that limits the allowable differences in z displacement for closely spaced points. What is interesting is how little difference in the autocorrelation function is needed to result in completely different looking surfaces. For example, Fig.5 shows the height image and the autocorrelation function of a 3m by 3m Gaussian surface whereas Fig.6 shows the height image and autocorrelation function of a similar sized power-law surface. The two surfaces can be easily distinguished by their visual appearance despite the autocorrelation function being quite similar especially at small lags.

D. Simulation results

The "cloud of points" model was used to simulate the backscattering of an incident sound wave off three sand-like simulated seafloors with three different roughness properties. All three seafloors were sampled at 2mm spacing in x and in y. The three different seafloors were: a flat granular surface covering 3m by 3m area and with random uncorrelated displacements of RMS roughness equal to $200\mu m$, a correlated Gaussian surface with a RMS roughness of 1cm and a correlated power-law surface with a similar 1cm RMS roughness averaged over the 3m by 3m area sampled. The last two surfaces, their autocorrelation functions and a slice through the 2-D power spectra are shown in Fig. 5 and Fig.6.

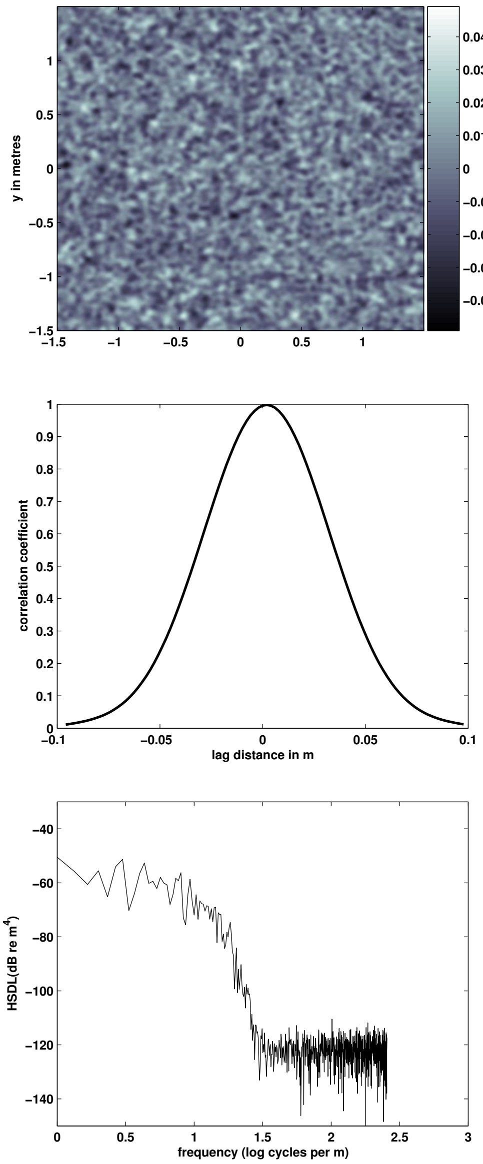

Fig. 5. (a) The height image of a Gaussian seafloor (b) its autocorrelation function and (c) a slice through the 2-D power spectrum.

An omni-directional projector/hydrophone was suspended 0.5m above the simulated seafloor such that the first arrival time for an impulse transmitted at t=0 would be 0.667ms. The first results shown are the reflections we would expect from a "perfect mirror". This test is essential to check the import of the seafloor sampling interval; in our case 2mm. Using the discrete equivalent of the Kirchhoff-Fresnel integral,

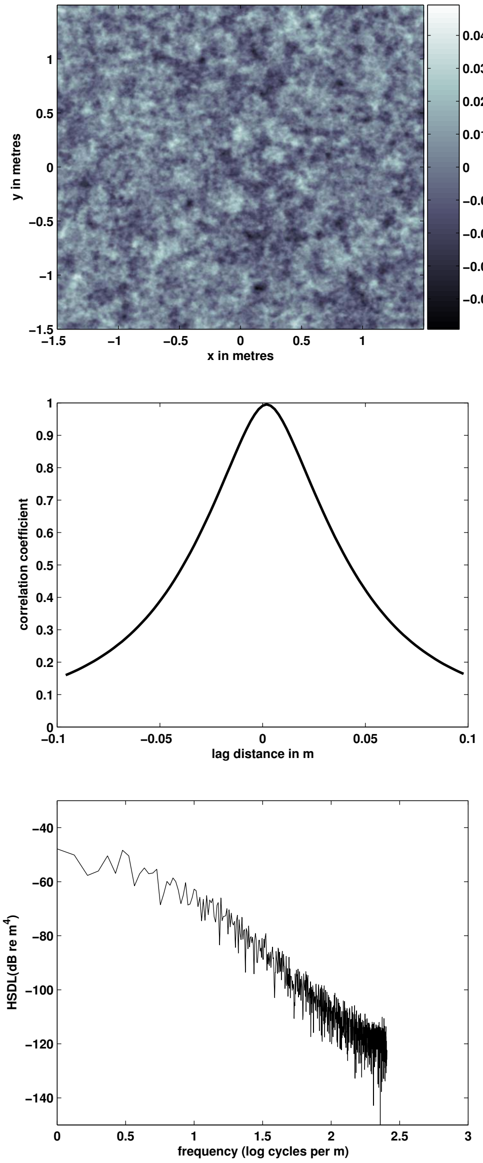

Fig. 6. (a) The height image of a power law seafloor, (b) its autocorrelation function and (c) a slice through the 2-D power spectrum

we compute the frequency response up to 500kHz and the amplitude spectrum is shown in Fig.7(a). Note that after about 400kHz, aliasing sets in. What is interesting is that the errors injected by aliasing only effect the channel impulse response after 1ms as can be seen in Fig.7(b). Thus we could either window out all frequencies above 400kHz or limit the time window to less than 1ms. We have chosen the former which means the channel impulse response is broadened but there is no time limit imposed. The window is a three-term Blackman-Harris window out to 400kHz and the (re-scaled) windowed spectrum is show in Fig.8(a) with its corresponding impulse response shown in Fig.8(b). Note that the spectrum has just a hint of aliasing and the impulse response is clean out beyond 2ms where impulses from the edges of the 3m by 3m seafloor start to arrive at 2.1ms.

Since the windowed amplitude spectrum encompasses 0Hz (equivalently $k = 0$), it is interesting to see the effect of approximating $(jk + 1/r)$ by jk inside the integral. Fig.9(a) shows a zoomed in section of the frequency windowed impulse response with the response that would be obtained by a perfectly flat mirror surface. Without $1/r$ inside the integral, an error is injected into the time response as shown in Fig.9(b). In most situations this does not matter as $S(f)$ for real transducers seldom has any response down at low frequencies so although the channel impulse response $h(t) = \mathcal{F}^{-1}\{H(f)\}$ may be slightly in error by dropping the $1/r$, the echo $e(t) = \mathcal{F}^{-1}\{E(f)\}$ is not.

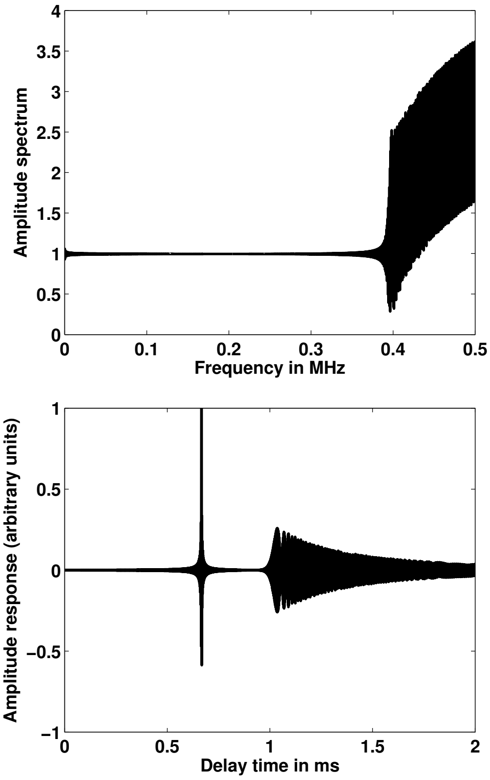

Fig. 7. The results from a 3m by 3m mirror surface computed using a discrete approximation to the Kirchhoff-Fresnel integral. (a) The full amplitude spectrum $|H[f]|$ up to a frequency of 0.5MHz. Notice the aliasing errors that occur above a frequency of 0.4MHz. (b) The channel impulse response $h[t]$ showing the effects of aliasing errors.

Now a perfectly flat, sandy seafloor is not a mirror and so the first seafloor to be simulated is where every seafloor sample has a small random vertical displacement by an uncorrrelated Gaussianly distributed amount which has an RMS value of 200μm. Hopefully this is a good model for "fine sand" with a ϕ value of 2.25 [4] , p200. If we assume the gains are spherical and well-sorted there would be on average 10 grains between seafloor samples so the displacements are unlikely to have any significant correlation from sample point to sample point. This in many ways in analogous to the "noise floor" in a communication system.

When the flat granular surface is replaced by a rough surface with a Gaussian autocorrelation function, interference becomes evident in the spectrum and the corresponding channel impulse

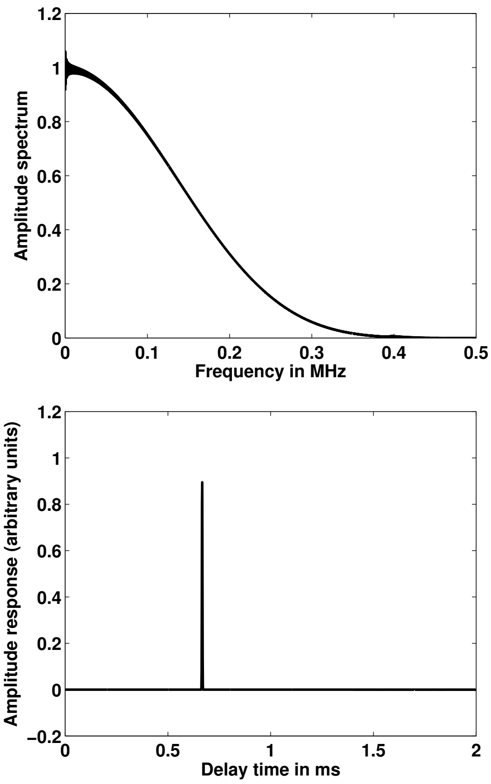

Fig. 8. The results from a 3m by 3m mirror surface after a Blackmann-Harris windowing of $H[f]$ to remove aliasing errors. (a) The windowed amplitude spectrum. Note the vertical scale has been changed from Fig.7a. (b) The corresponding channel impulse response.

response shows an earlier, slightly slower, rising edge with a significant extension into the trailing edge. Although the detailed structure of every echo will be different, they still follow the same expected envelope.

The spectrum and impulse response of the power-law surface, Fig.10, shows the amplitude spectrum is more sharply "modulated" and a similar bipolar channel impulse response with the tail of the impulse response lasting slightly longer than that from the Gaussian surface.

At first sight, the channel impulse response Fig.10(b) appears to be in error with a significant number of negative going impulses in time waveform which is a puzzle considering the transmitted signal illuminating the surface is a single positive-only impulse (i.e., $s(t) = \delta(t)$). However this apparent error is discounted when it is realised that the equivalent time domain summation to the KFI over the surface samples is that of many delayed replicas of the differential of the transmitted signal which of course has both positive and negative excursions from the mean.

Of course none of the channel impulse responses is directly observable since the spectrum of the echoes received by the hydrophone is weighted by $S(f)$ (or for the frequency sampled case $S[f]$) which does not go down to 0Hz or much above 100kHz for the transducer set we are using in the simulation. So what would be seen if the seafloor was a mirror? Clearly we would measure a near perfect replica of the transmitted waveform $s[t]$ delayed by in our case by 0.667ms.

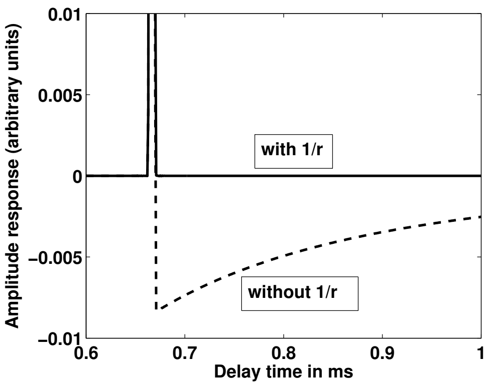

Fig. 9. The fine-scale details of the channel impulse response of the windowed spectrum from a 3m by 3m mirror using $(jk + 1/r)$ inside the integral as given by (3)— the solid line and using the approximation (jk)— the dotted line. (Note both the time scale and the amplitude scale have been expanded from the previous figure.)

The spectrum $S[f]$ is shown in Fig.11(a) and the delayed echo $s[t - 2z/c]$ in Fig.11(b). When the mirror is replaced by a globally flat but granular seafloor, there is little visual difference between $|S[f]|$ and $|E[f]|$ or between $s[t - 2z/c]$ and $e[t]$. The most that could be seen is some minor ripples in $e[t]$ after 0.75ms. Of course a real seafloor would have reflection coefficient less than 1.0 so there would be some extra amplification needed in the receiver circuits so that direct comparisons could be made.

The plots are radically different when the flat seafloor is replaced by the rough Gaussian seafloor. There is now interference in the spectrum and the pulse echo has a much more gradual rise time in the leading edge of the envelope and the falling edge of the envelope is extended out to beyond 1ms. Similar effects are seen with the rough power-law seafloor as shown in Fig.12.

How the channel pulse echo return changes with sonar position is of significant interest since techniques such as synthetic aperture sonar rely heavily on significant correlation from ping to ping as the sonar head moves down the track. (As a matter of semantics we call the modulated transmitted waveform $s(t)$ a ping whereas a delta function transmitted waveform $\delta(t)$ a shot.) Figure 13 shows the close range results for 40 pings. The upper image shows the intensity of the pings as the sonar moves and pings every 10mm along track. The clear trace around 0.7m range is of interest since it clearly demonstrates that the position of closest approach (around ping 270) is not the position of strongest return; that occurs around ping 240. Our assumption then is that the seafloor at this position must be tilted around the horizontal.

IV. Discussion

Our motivation for using this simulation model is to investigate the feasibility of using a synthetic aperture sonar in extremely shallow waters. The specific result that interest us most is how the phase of a target in the field of view evolves from ping to ping as the sonar tracks over the rough seafloor. Since the maximum range is so small—less than 5m—a single projector-hydrophone is sufficient (rather than the single

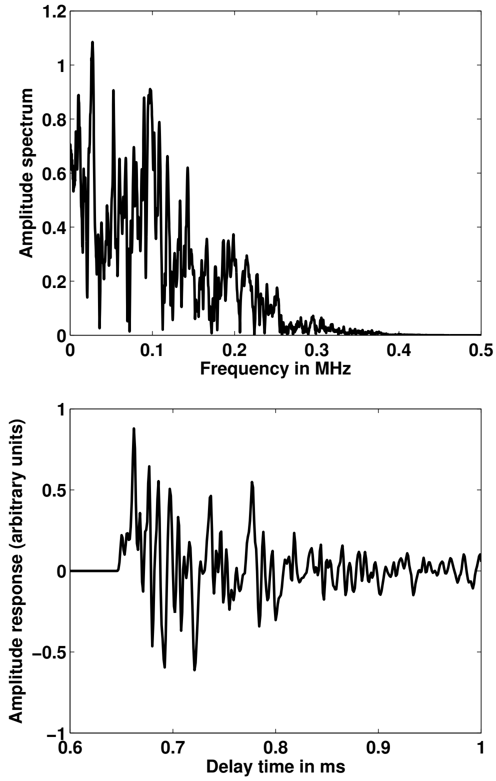

Fig. 10. The broad-band returns for one example of a granular power-law surface with grain size of $200\,\mu$m, RMS roughness of 1 cm measured over a 3 m by 3 m area and shown in Fig.6. (a) A typical windowed amplitude spectrum, $|H[f]|$. (b) The early details of a typical channel impulse response, $h[t]$. These plots should be compared to thios presented in Fig. 8.

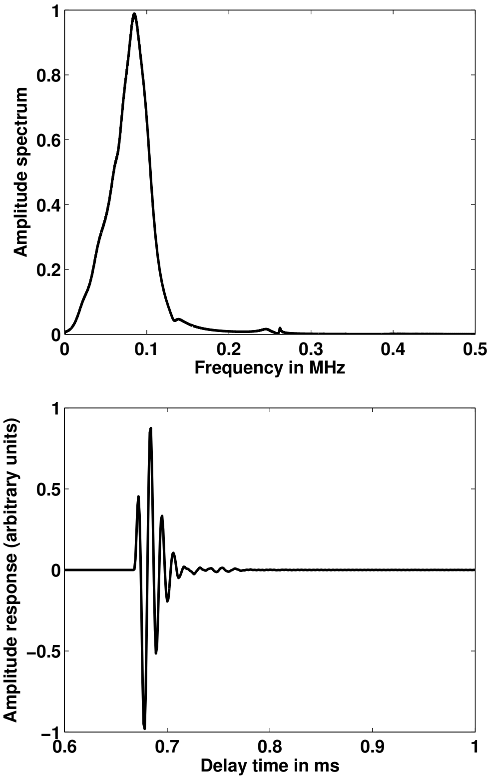

Fig. 11. The narrow-band pulse-echoes for a 3m by 3m mirror surface with (a) The amplitude spectrum $|S[f]|$. (b) The early details of the pulse-echo time response $s[t - 2z/c]$.

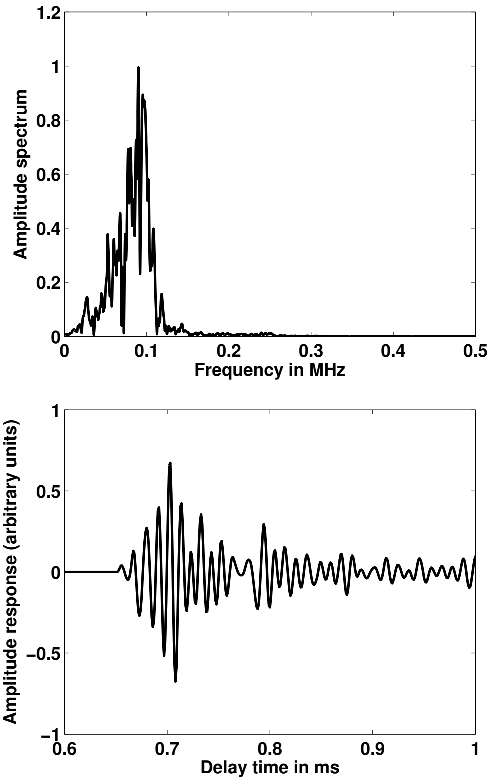

Fig. 12. The narrow-band pulse echoes for one example of a granular power-law surface with RMS roughness of 1cm over the 3m by 3m aperture and the surface is shown in Fig.6. (a) A typical amplitude spectrum $|E[f]|$. (b) The early details of a typical pulse echo time response $e[t]$.

projector-multiple hydrophone array that has become standard for deeper water SAS).

Clearly a shallow water SAS would use a more directional transducer set rather than the hemispherical transducers we have simulated here. However the hemispherical transducers represent close to a worst case scenario for multipath impairments so a basic understanding of how the seafloor roughness changes the phase history can still be determined.

One aspect of the seafloor reverberation modeling we have completely ignored is the volume scattering inside the sediment. If the shallow water SAS is intended to image buried targets, the scattering from the volume around the target will need to be included in the total reverberation masking the signal [10] [11].

One well-known disadvantage of the KA model of surface scattering is that it overestimates the target strength at small grazing angles and clearly a shallow water SAS will be used at small grazing angles. So the question might be asked why not use the small slope approximation (SSA) model which does as well as the KA for large grazing angles but does not overestimate the target strength at small grazing angles. In Appendix I it can be shown that for a plane incident wave, a simple correction factor can be applied to the echo returns from small grazing angles which compensate for this overestimation and produce similar results to the SSA without

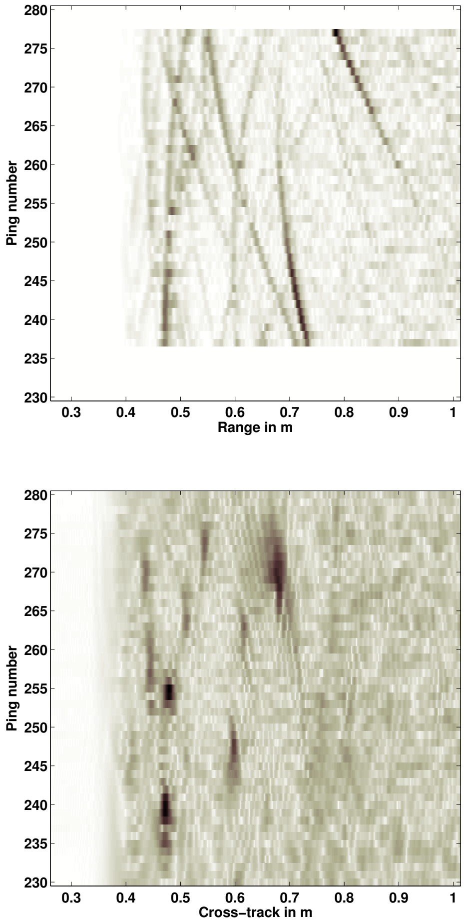

Fig. 13. (a) The raw data from 40 pings showing $|s[t]|$ as a function of ping number and (a) the SAS image reconstructed.

needing to employ the full SSA model which is significantly more complicated than the KA approach.

V. Conclusions

The Kirchhoff-Fresnel diffraction integral (KFI) is an excellent starting point for simulation of seafloor reflection and scattering. By starting out with a sampled but perfectly reflecting flat mirror surface, any aliasing problems can be identified to ensure the balance between surface sampling distance and time sampling period is appropriate. Once the effects of aliasing has been eliminated by suitable windowing of the spectrum of the echoes, the impulse responses and echoes for various seafloor realizations can be computed and so compared. Since this is a full 3-D simulation, sea-floors with anisotropy can be investigated quite easily.

Simplification of the computations by dropping the 1/r term inside the integral effects the channel impulse response $h[t]$ but not the echoes $e[t]$ provided the spectral weighting of the transducer set $S(f)$ does not go down to 0Hz which is the norm for real physical transducers.

Although this has not been done in this paper, the effect of surface shadowing at smaller grazing angles can be added if required and this may be necessary as the roughness increases. Also the KA is known overestimate the backscattering from a rough seafloor at small grazing angles but a simple angular dependent correction factor can be applied which compensates for this overestimation and brings the backscattered target strength into line with what would have been calculated using the more accurate SSA.

The model we propose here is well suited to small areas of seafloor (in our case 3m by 3m) but the computing load increases rapidly with area. Large areas and blocky objects with sharp corners and edges are better simulated with the larger rough facet approach.

Volume scattering (i.e., reverberation originating from within the sediment) will need to be added to calculate a more complete pulse-echo response. Whether this is numerically feasible depends of the type of volume scattering. If it is a result of large scale density or speed of sound inhomogeneities in the sediment, then the voxel count may not be too large. However if the scattering is a result of shells or stones buried in the sediment then the voxel size could well need to be 1mm by 1mm by 1mm. Modeling a seafloor of 3m by 3m down to a depth of say 50mm would require more computing power than most researchers have available.

One of the most interesting aspects of this modelling is that the reconstructed SAS image looks nothing like the actual surface even allowing for the visual effects of side lighting. This is in stark contrast to SAR where the reconstructed SAR image looks like a distorted but recognisable aerial photograph.

References

[1] A. J. Hunter, M. P. Hayes and P. T. Gough, Fast Fourier-domain modelling fro a SAS simulator with application to time-variant targets, aspect dependent occlussions and Doppler efffects,*IEEE Oceans'06 Asia-Pacific* Singapore, May 2006

[2] E. I. Thorsos, The validity of the Kirchhoff approximation for rough surface scattering using a Gaussian roughness spectrum *J. Acoust. Soc. Am*, **83**(1), 1988: 78–92.

[3] E. I. Thorsos, Acoustic scattering from a “Pierson-Moskowitz” sea surface. *J. Acoust. Soc. Am*, **88**(1), 1990: 335–349.

[4] D. R. Jackson and M. D. Richardson, *High frequency seafloor acoustics*, Underwater Acoustics Series, New York, USA: Springer, 2007.

[5] C.M.McKinney and C. D. Anderson, Measurements of backscattering of sound from the ocean bottom, *J. Acoust. Soc. Am*, **36**(1), 1964: 158–163.

[6] O. George and R. Bahl. Simulation of backscattering of high frequency sound from complex object and san sea-bottom. *IEEE J. Oceanic Eng.*, **20**(2), 1995: 119–130.

[7] S. L. Broschat and E. I. Thorsos, An investigation of the small slope approximation for scattering from rough surfaces. Part II. Numerical studies. *J. Acoust.Soc.Am*, **101**(5), 1997: 2615–2625.

[8] H. J. Camin, *A comparison of spherical wave sediment reflection coefficient measurements to plane wave models*, MSc Thesis, University of Texas at Austin, 2004.

[9] C. Vernold and J. E. Harvey, A modified Beckmann-Kirchoff scattering theory for non-paraxial angles, *SPIE Conf. on Scattering and Surface Roughness*, **3426**, 1998: 51–56.

[10] E. Pouliquen, O. Bergem and N. G. Pace, Time-evoluion modeling of seafloor scatter, . Concept *J. Acoust. Soc. Am*, **105**(6), 1999: 3136–3141.

[11] O. Bergen, E. Pouliquen, G. Canepa and N. G. Pace, Time-evoluion modeling of seafloor scatter, . Concept *J. Acoust. Soc. Am*, **105**(6), 1999: 3142–3150.